Journal of Power Sources 199 (2012) 68–74

Contents lists available at SciVerse ScienceDirect

Journal of Power Sources

journal homepage: www.elsevier.com/locate/jpowsour

The application of Ir–V/C catalyst as a durable anode catalyst for a 1.5 kW proton exchange membrane fuel cell stack

Daijun Yang[a,b], Bing Li[a,b], Hao Zhang[a,b], Junsheng Zheng[a,b], Rui Lin[a,b], Jianxin Ma[a,b,*]

[a] Clean Energy Automotive Engineering Center, 4800 Caoan Road, Tongji University, Shanghai 201804, China
[b] School of Automotive Studies, 4800 Caoan Road, Tongji University, Shanghai 201804, China

ARTICLE INFO

Article history:
Received 31 July 2011
Received in revised form 10 October 2011
Accepted 11 October 2011
Available online 15 October 2011

Keywords:
Anode
Catalyst
Ir–V/C
Stack
Durability

ABSTRACT

Ir–V nanoparticles are prepared with a modified ethylene glycol (EG) reduction method and use as anode catalyst for a 15 cell, 1.5 kW proton exchange membrane fuel cell (PEMFC), with the main purpose of verifying the durability of the as-prepared catalyst. Polarization curves, line scan voltammograms (LSVs), and cyclic voltammograms (CVs) show that the 40% Ir–10% V/C anode is of comparable performance with a commercial Pt/C anode. After a 1010 h driving cycle test, the stack exhibits a minor degradation rate of 1.2% at rated power. The resulting performance and durability of the fuel cell stack demonstrate the as-prepared catalyst has the potential to be used in PEMFC.

© 2011 Elsevier B.V. All rights reserved.

1. Introduction

The progress of proton exchange membrane fuel cell (PEMFC) has a history of cost-reduction. PEMFCs did not receive much attention from government agencies or industries until a couple of decades ago when breakthrough methods for reducing the amount of Pt, the most effective catalyst and expensive metal used in both the cathode and anode, were invented and developed. Notably, by virtue of the catalyst-ink technique, the utilization ratio of Pt has been tremendously increased, and its loading was reduced from tens of mg cm^{-2} to less than 1 mg cm^{-2} [1]. After the revival of the PEMFCs, its major application has been focused on transportation, primarily because of its high efficiency and environmental benignancy. The major barriers currently preventing PEMFCs from successful commercialization are the high cost and insufficient durability [2]. Fortunately, the manufacturing expenses are believed to be substantially decreased when moving from prototype to mass production, as predicted by the US Department of Energy (DOE) [3]. However, the cost of Pt will definitely grow with an increase in the production of these fuel cells due to its scarcity. This problem can only be resolved by further decreasing Pt loading, which has been decreased by two orders of magnitude of Pt has been reduced over the past decades [4], or using non-platinum catalysts as a long-term resolution [5,6]. Recently, tremendous progress has been achieved in both the activity and stability of non-platinum cathode catalysts [7–9]. However, due to the smaller amounts of Pt used at the anode, the replacement of platinum and platinum alloys with respect to the anode side have not been investigated extensively. Serov and Kwak [10] conducted an extensive review on the performance and potential of non-platinum anode catalysts, focusing on transition metal carbides, oxides, and alloys. When considering performance, it is of extreme importance that these anode non-Pt catalysts meet the lifetime target set by the DOE, which is prescribed to be 5000 h by 2010/2015 [11].

As for non-Pt catalyst, Ir and its oxides and alloys have been proposed as substitutes or promoters for Pt at the cathode because of their excellent oxygen evolution, high activity, strong affinity for OH or O species and stability in acidic media [12]. Very good performances have been achieved in ethanol oxidation on an Ir–Sn [13] catalyst in direct ethanol fuel cells (DEFCs) and formic acid oxidation on a Pd–Ir [14] catalyst in direct formic acid fuel cells (DFAFCs); in addition, Ir–Se [15] and Ir_xCo_{1-x} [16] methanol tolerances for oxygen reduction and oxygen reduction on $Ir_{85}Se_{15}$/C [17], IrO_2/Ti, and IrM (M = Ru, Mo, W, V) O_x/Ti binary oxide electrodes have been promising [18]. Very recently, our group found that an Ir–V/C catalyst showed excellent catalytic activity both for hydrogen oxidation reaction (HOR) [19] and oxygen reduction reaction (ORR) [20]. Unfortunately, the Ir–V/C catalyst durability has not been studied in these works. In order to further address this issue, in the present work, we adopted a strategy to synthesize electrocatalysts based on Ir and the co-catalytic metal V, with a focus

* Corresponding author at: School of Automotive Studies, 4800 Caoan Road, Tongji University, Shanghai 201804, China. Tel.: +86 21 6958 9480; fax: +86 21 6958 3850.
E-mail addresses: jxma@tongji.edu.cn, jxma@tongji.edu.cn (J. Ma).

0378-7753/$ – see front matter © 2011 Elsevier B.V. All rights reserved.
doi:10.1016/j.jpowsour.2011.10.035

Table 1
Optimized PEMFC stack operation conditions.

Pressure (A/C)	Stack coolant		Humidification (dew point)		Flow stoichiometry	
	Flow	Outlet temperature	H_2	Air	H_2	Air
0.2 bar/0.3 bar	15 l min^{-1}	≤73 °C	77 °C	80 °C	1.5	2.8

on durability and performance. As an alternative for Pt/C, the as-prepared Ir–V/C was used as anode catalyst for a 1.5 kW FC stack, and a 1010 h durability test was conducted to elucidate its ability to meet the criteria for automotive applications.

2. Experimental methods

2.1. Materials

All chemicals used for preparing the catalyst preparation were reagent grade and included the following: iridium chloride hydrate [$IrCl_3{\cdot}6H_2O$], ammonium metavanadate [NH_4VO_3], isopropanol, ethylene glycol, sodium hydroxide [NaOH] and hydrogen chloride [HCl] (Sinopham). Pure H_2 and N_2 were supplied by Shanghai Research Institute of Chemical Industry. All solutions were prepared using deionized water purified with a water purification system (Model R30, Purelab). The resistivity of the deionized water was above 18 MΩ cm. Carbon black supplied by Cabot Corporation (Vulcan XC-72, SBET = 236.8 m^2 g^{-1}) was used as a support. 40% Pt/C (Johnson Matthey) was employed as standard cathode catalyst, while 5 wt.% Nafion® solution and proton exchange membrane (N212) were provided by DuPont.

2.2. Catalyst preparation

Carbon-supported Ir–V nanoparticle catalysts were prepared via a modified ethylene glycol (EG) method. Iridium chloride and ammonium metavanadate were mixed with carbon black in ethylene glycol, and then the mixture was ultrasonicated and stirred for 4 h to obtain an "ink". A 2 M NaOH solution was added into the ink to adjust the pH of the ink to 12. Meanwhile, excess ethylene glycol was added into the ink to completely reduce the metal ions. The mixture was stirred and refluxed at 120 °C for ca. 3 h. During this process, the pH value was monitored and adjusted to 3 by adding 5 M HCl before cooling the mixture to room temperature. The resulting powder was filtered, washed with deionized water until the $AgNO_3$ precipitated the Cl^-, and then dried at 70 °C for 2 h. The dried catalyst powder was treated at 200 °C in a tube furnace under an atmosphere of N_2 and H_2 (9:1, vol:vol) for 2 h. Detailed information about the effect of the pH on catalyst performance can be found in our previous work [21]. The 40% V/C catalyst was prepared with the same procedure mentioned above.

2.3. Characterization of the catalyst

X-ray diffraction (XRD) measurements of the catalysts were performed on a PHILIPS PW 3040/60 powder diffractometer using Cu Kα radiation (λ = 1.541 Å). The diffractometer was operated at an accelerating voltage of 40 kV, a beam current of 40 mA, and a temperature of 25 °C. The data were collected in the 2θ range of 10–100° and at a scan rate of 1.20° min^{-1} and processed using the JADE5 software. The morphologies of the catalysts before and after the durability test were observed using a transmission electron microscope (TEM) (model JEM 2010, JEO) operated at 200 kV.

2.4. Linear scan voltammogram (LSV) and cyclic voltammogram (CV).

LSVs and CVs were recorded in an electrochemical cell using Ag/AgCl as a reference electrode and Pt foil as a counter electrode at room temperature. All measurements were performed in a 0.5 M H_2SO_4 solution and flushed with pure H_2 or N_2. To prepare the working electrode, the as-prepared catalyst ink was sprayed on to a rotating disk electrode (RDE) (Model AFMSRCE, Pine). The rotation speed of the RDE was 300 rpm. The HOR activities of the catalysts were evaluated by employing this rotation system in a potential range of −0.27 to −0.96 V in the positive direction at a scan rate of 5 mV s^{-1} for LSV measurements and −0.27 to −1.16 V at a scan rate of 50 mV s^{-1} for CV measurements.

2.5. Fabrication of membrane electrode assemblies (MEAs)

MEAs with non-platinum catalysts and an active area of 250 cm^2 were fabricated as follows: the as-prepared 40% Ir–10% V/C powder was mixed with 5 wt.% Nafion® and isopropanol under stirring (Model B25, BRT) for 20 min to obtain the anode ink, and the ratio of metal to Nafion® polymer was maintained at 3:1 (in weight). The ink was then directly spayed onto one side of an N212 membrane at 90 °C using an automatic spraying system (Model Exacta Coat FC, SonoTek) to produce the anode. The cathode was prepared in the same procedure, i.e., spraying the cathode ink of 40 wt.% Pt/C onto the other side of the membrane. The loading of Ir and Pt on the catalyst-coated membrane (CCM) was the same (0.4 mg cm^{-2}). An MEA was then assembled by physically placing a gas diffusion layer (GDL) (Model 25 BC, SGL) on each side of the CCM, without hot pressing. A 15-cell, 1.5 kW stack was fabricated using such MEAs and graphite bipolar plates (BPPs).

2.6. Stack durability test

The stack was run on a FC test station (FCT, Inc.). Prior to driving cycle operation, we pre-tested the stack under different operating conditions to obtain the optimal parameters, which are listed in Table 1.

Under these operating conditions, a dynamic load derived from the actual FCV drum test data based on the J1015 driving cycle was imposed on the stack. The profile of the dynamic load is shown in Fig. 1, where the output current density, instead of vehicle speed, is directly reflected. It can be seen that the load period was 620 s, and the peak load during each cycle was 660 mA cm^{-2}. Noticeably, at the end of the cycle, a full throttle acceleration scenario is imposed to test the quick response capability of the stack. It is critical and reasonable to choose such a dynamic load cycle profile because fuel cell stacks designed for vehicles are often reported to have poorer lifetime expectancies than under constant load conditions [22]. Dynamic load cycling can approach a real situation of FCV and therefore reasonably reflects the durability of a stack in real world applications.

The 1.5 kW stack was run for at least 12 h each day and re-started after fully cooling down to examine its start–stop performance and its impact on the durability of the stack.

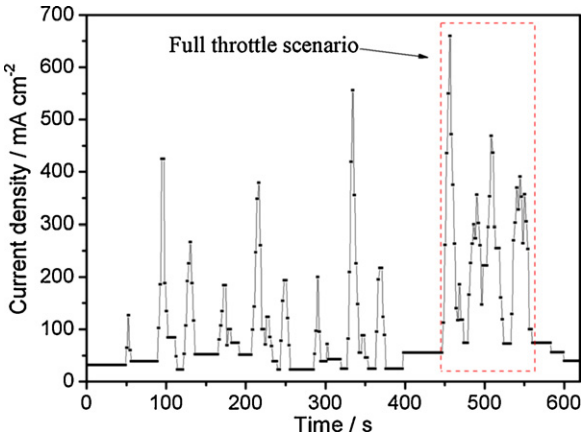

Fig. 1. Profile of dynamic load cycle used for durability test.

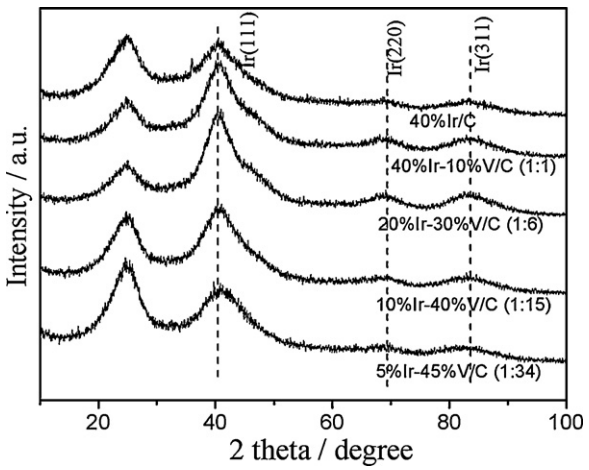

Fig. 2. XRD patterns of 40% Ir/C and Ir–V/C at different atomic ratios.

Power as a function of the real time (*P*–*t*) was recorded, while polarization (*V*–*I*) measurements were conducted once a day. Following each polarization curve test, electrochemical impedance spectrum (EIS), another useful in situ approach, was employed to depict the performance change of the whole stack. Nyquist plots were measured via an impedance testing system (Model KFM2150, Kikusui) at 100 mA cm^{-2} with 6 points per decade of a frequency scan range from 10 kHz to 100 mHz. The stack was run at 75 °C and ambient pressure with air flowing through the cathode (working electrode) and hydrogen flowing through the anode (counter electrode) [23]. The counter electrode was also used as the reference electrode.

3. Results and discussion

Fig. 2 shows the XRD patterns of the as-prepared 40% Ir/C catalyst and the Ir–V/C catalysts at different atomic ratios; 40% Ir–10%

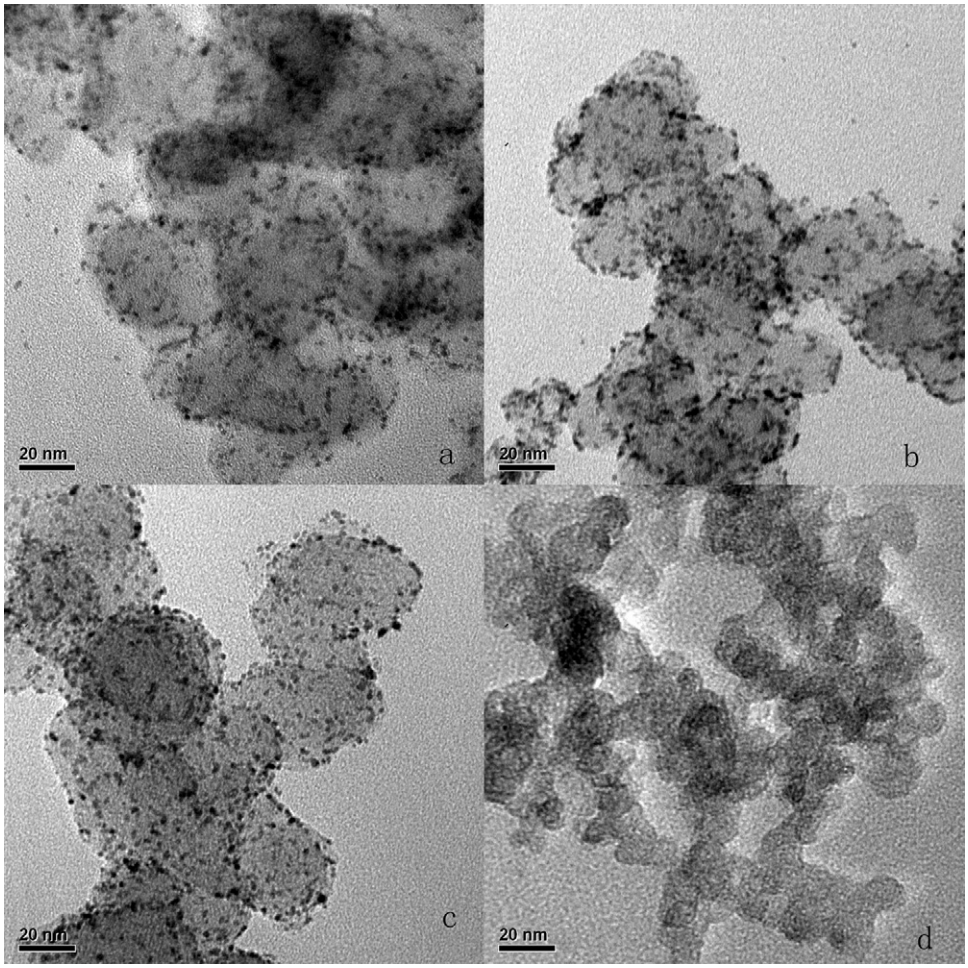

Fig. 3. TEM images of the (a) Ir/C and Ir–V/C nanoparticles prepared with different atomic ratios of Ir and V; (b) 1:6 (20% Ir–30% V/C); (c) 1:15 (10% Ir–40% V/C); (d) 1:34 (5% Ir–45% V/C).

Table 2
Atomic ratio effect on the structural parameters of Ir/C and Ir–V/C catalysts from XRD results.

Catalyst	Atomic ratio of Ir to V	Ir(2 2 0) peak position (°)	Lattice constant *A* fcc (Å)	Particle size (nm)
40% Ir/C	–	68.66	3.866	3.3
40% Ir–10% V/C	1:1	68.98	3.856	2.7
20% Ir–30% V/C	1:6	69.17	3.855	2.4
10% Ir–40% V/C	1:15	69.39	3.853	1.9
5% Ir–45% V/C	1:34	69.42	3.851	0.81

V/C (1:1), 20% Ir–30% V/C (1:6), 10% Ir–40% V/C (1:15) and 5% Ir–45% V/C (1:34). Each pattern shows three peaks at about 40.30°, 69.02°, and 83.73°, corresponding to the face-centered cubic (fcc) crystallinity of Ir particles in the Ir/C catalysts. The peak at 25° can be ascribed to the diffraction of the (0 0 2) plane of carbon black particles. No peaks related to V and its various oxides [24] were observed in the XRD patterns. It is believed that the co-catalytic metal V leached out through the addition of HCl in the catalyst preparation process, leaving behind a coarsened surface of Ir clusters, which may account for the performance enhancement [25,26]. The average size of the Ir particles in Ir/C and Ir–V/C was calculated according to Scherrer's equation [27]. The resultant structural parameters, including the Ir(2 2 0) peak position, lattice constant and the average particle size, are listed in Table 2. The results show that the mean particle size decreased from 2.7 nm for Ir–V/C (1:1) to 2.4 nm and 1.9 nm for Ir–V/C (1:6) and Ir–V/C (1:15), respectively. In other words, the introduction of V to Ir/C may decrease the lattice constant of the Ir(fcc) crystal, which induces a shift in the Ir(2 2 0) reflection peak to a higher position with decreasing atomic ratios. When the atomic ratio was further decreased to 1:34, the Ir nanoparticles became so fine that the diffraction peak of Ir(2 2 0) almost disappeared, such that the corresponding lattice constant and even the average particle size could not be definitely calculated; however, the presence of Ir cannot be disregarded because it may be present in a very small amount. These results indicate the importance of controlling the atomic ratio of Ir and V on the particle size and fcc of Ir–V/C electrocatalysts. The possibility of H_2 adsorption and splitting on Ir atoms may increase as the lattice constant decreases. The Ir–Ir distance in Ir–V/C catalyst is shortened, and H_2 can then easily be adsorbed on Ir, thus accelerating H–H bond breaking. Therefore, the activity of Ir/C may be enhanced by the addition of V through the strengthened Ir–H bond. The TEM images of the Ir/C and Ir–V/C catalysts at different atomic ratios [20% Ir–30% V/C (1:6), 10% Ir–40% V/C (1:15) and 5% Ir–45% V/C (1:34)] are displayed in Fig. 3. By decreasing the atomic ratios of Ir and V in catalyst synthesis, the average particle size decreased.

The typical CVs of the 40% Ir–10% V/C, 20% Ir–30% V/C, 10% Ir–40% V/C, and 5% Ir–45% V/C catalysts immediately after deposition on the RDE are shown in Fig. 4. The potential range between 20 and 200 mV during the forward scan reveals that, except for 5% Ir–45% V/C, the Ir-based nanoparticle catalysts have comparable hydrogen adsorption/desorption charges. The narrow adsorption/desorption potential range suggests excellent HOR activity. Compared to pure Ir/C catalyst, the leaching of V from the catalyst surface leads to a higher active surface area for HOR. As a result, HOR reactivity is significantly influenced when the ratio of Ir:V was decreased to 1:34.

For further determination of the optimal ratio of Ir:V, LSVs shown in Fig. 5 were used. 40% Ir–10% V/C exhibited the best HOR activity under a lower potential scan rate. At a scan rate of 5 mV s^{-1}, which is 10% of that used in the CV experiments, the kinetic activities of the catalysts were manifested and compared. The oxidation current of 40% Ir–10% V/C was much higher than those of the other catalysts, e.g., approximately 2.0 and 3.2 times of 5% Ir–45% V/C and 40% Ir/C at 0.1 V, respectively. The current-voltage curves for a single PEM fuel cell under H_2/air conditions using Ir and Ir–V/C

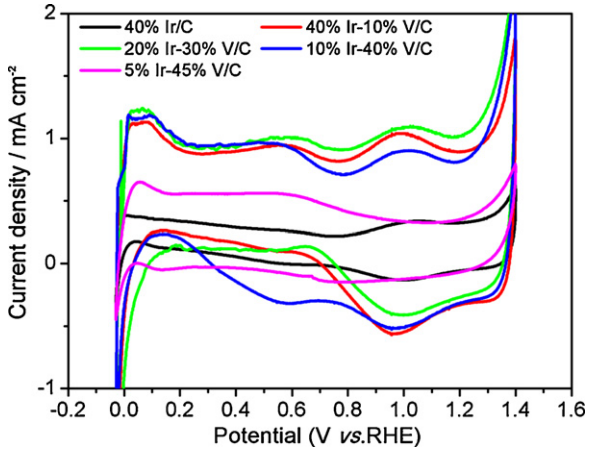

Fig. 4. Cyclic voltammograms for H_2 on Ir/C, Ir–V/C with different Ir:V ratios in 0.5 M H_2SO_4 at the ambient solution temperature in H_2; Rotation speed: 300 rpm, scan rate: 50 mV s^{-1}, electrode area: 0.283 cm^2; catalyst loading: 28 μg cm^{-2}.

as anode electrocatalysts were investigated. In Fig. 6, the fuel cell with 40% Ir–10% V/C (1:1) as the anode catalyst had the best performance. This strongly suggests that more catalyst active sites could be achieved due to the modification of Ir with V, which greatly reduces the activation polarization. This behavior is attributed to the amount of catalyst per geometric area available to reactant gases and thus electrochemically active in each dispersion. A very high power density was obtained even when the atomic ratio of Ir and V in the Ir–V/C catalyst decreased to 1:34. Here, about 1.5 times higher power density was obtained for 5% Ir–45% V/C (1:34) than that for pure 40 wt.% Ir/C. It can also be seen that the performances of the MEAs strongly depend on current density, suggesting an influence of the catalyst layer morphology and mass transport effects. Based on above results, 40% Ir–10% V/C was selected as

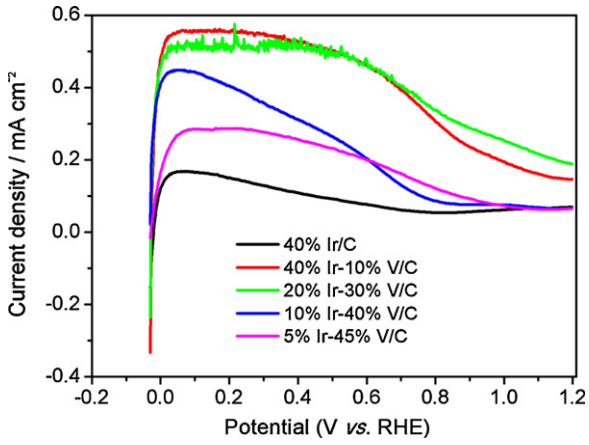

Fig. 5. Linear scan voltammograms for H_2 on Ir/C, Ir–V/C with different Ir:V ratios in 0.5 M H_2SO_4 at the ambient solution temperature in H_2; rotation speed: 300 rpm, scan rate: 5 mV s^{-1}, electrode area: 0.283 cm^2; catalyst loading: 28 μg cm^{-2}.

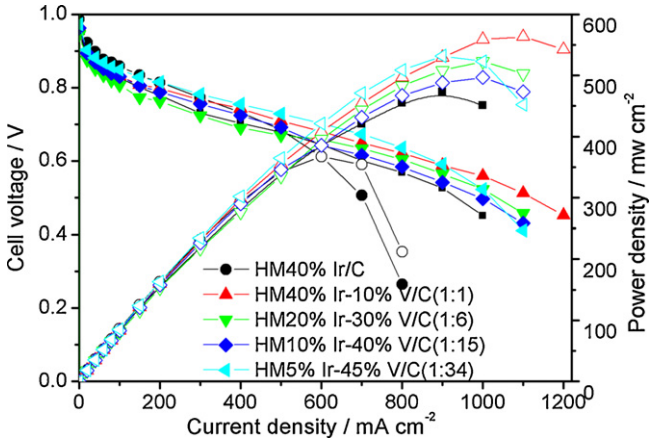

Fig. 6. Performance curves for Ir/C and Ir–V/C anode prepared at different atomic ratios of Ir and V, 40% Ir/C (0.4 mg_{Ir} cm^{-2}), 1:1 (40% Ir–10% V/C, 0.4 mg_{Ir} cm^{-2}), 1:6 (20% Ir–30% V/C, 0.2 mg_{Ir} cm^{-2}); 1:15 (10% Ir–40% V/C, 0.1 mg_{Ir} cm^{-2}); 1:34 (4% Ir–45% V/C, 0.1 mg_{Ir} cm^{-2}).

an anode catalyst and used in the following stack fabrication and durability test.

The as-prepared stack was run discontinuously under the dynamic load cycling in the daytime and was stopped overnight or at least 2 h per day. The stack experienced about 57 start–stops during the whole test. As aforementioned, during the dynamic load, cycling polarization curves were measured once a day. The cell performance can be obtained from dividing the stack performance by the cell number, 15. In terms of the average cell voltage and power density, the stack durability expressed in an interval of ca. 200 h is shown in Fig. 7. From the results at 200 h, 400 h, 600 h, 800 h, and 1010 h, it can be seen that the performance of the 1.5 kW stack experienced a very slight decrease. After about 200 h of "activation", the stack became more stable, and higher performance was achieved in the following 810 h. During the 1010 h test, only a minor degradation rate was observed. The averaged maximum power density of single cells changed from 490.7 mW cm^{-2} at the start to 484.9 mW cm^{-2} at 1010 h, i.e., a degradation of only 1.2%/1010 h was detected, which was even lower than the 2010 target of US DOE (5%/1000 h) [28]. The slight performance decay was also attributed by the on-line *P*–*t* curve recorded along the driving cycle test shown in Fig. 8.

The average cell power in the stack varied during the 1010 h continuous operation (Fig. 8). A meaningful phenomenon can be seen from Fig. 8, where the performance of the stack during the durability test clearly declined on a single day but recovered after

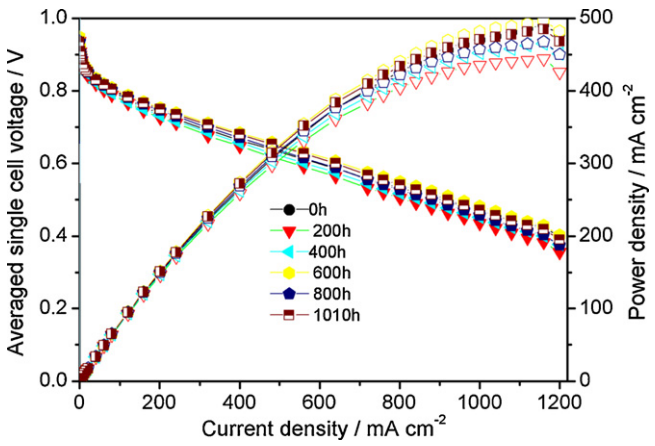

Fig. 7. Averaged cell performance of the PEMFC stack in 1010 h durability test.

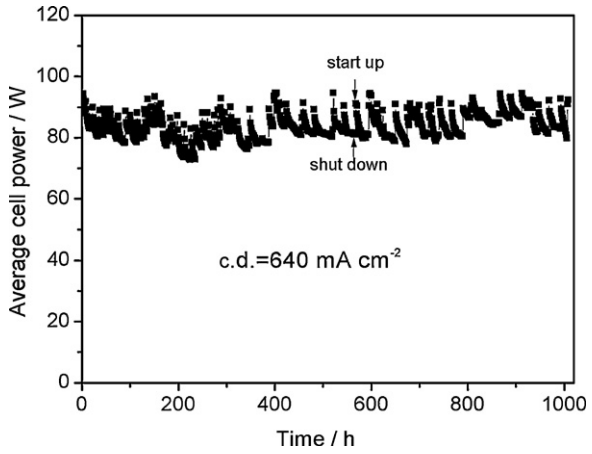

Fig. 8. Average cell power as a function of the operation time.

an overnight "rest". The performance degradation of the stack between every 2 days was minor. Therefore, we conclude that one night of "rest" of the stack led to the recovery of its performance.

In order to understand the change in structure of the anode catalyst particles, the particles after the 1010 h durability test were analyzed using the XRD technique, and the diffraction pattern is displayed in Fig. 9, where the pattern of the pristine catalyst is also included. In comparison with the pristine catalyst, a slight broadening of the diffraction peak for active carbon (0 0 2) plane was observed, which may be attributed to corrosion of the support during the dynamic loading test due to electrochemical and reverse water-gas reactions [29]. On the other hand, almost no observable changes in the position, broadening, or height of the peaks for the (1 1 1), (2 2 0), and (3 1 1) planes of the Ir particles were observed. Therefore, it can be concluded that the Ir–V/C catalyst possesses excellent stability because cycling the potential between the oxidation and reduction regions of a metal will lead to higher dissolution rates than just holding a potential in the oxidation region [30].

In addition, the TEM images characterized before and after the durability test in Fig. 10 show the average particle size of the pristine anode catalyst was 2.0 nm, consistent with the XRD result, and increased to 2.2 nm after the durability test. Fig. 10 also illustrates that the nanoparticles were uniformly dispersed on the surface of the carbon supports. Such a small increase in particle size and the absence of aggregation after the 1010 h dynamic load test may account for the tiny performance loss of the stack.

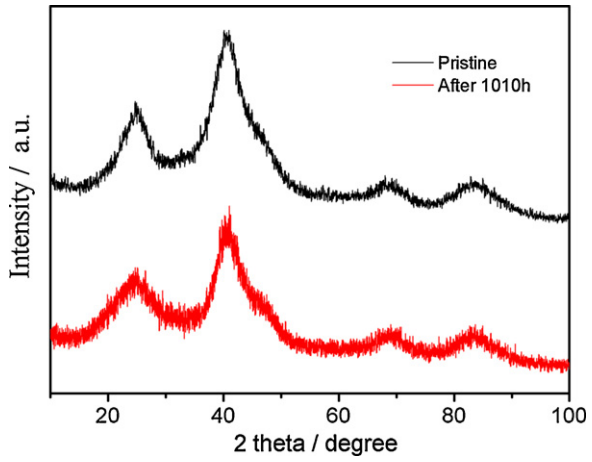

Fig. 9. XRD patterns of anode 40% Ir–10% V/C before and after 1010 h testing.

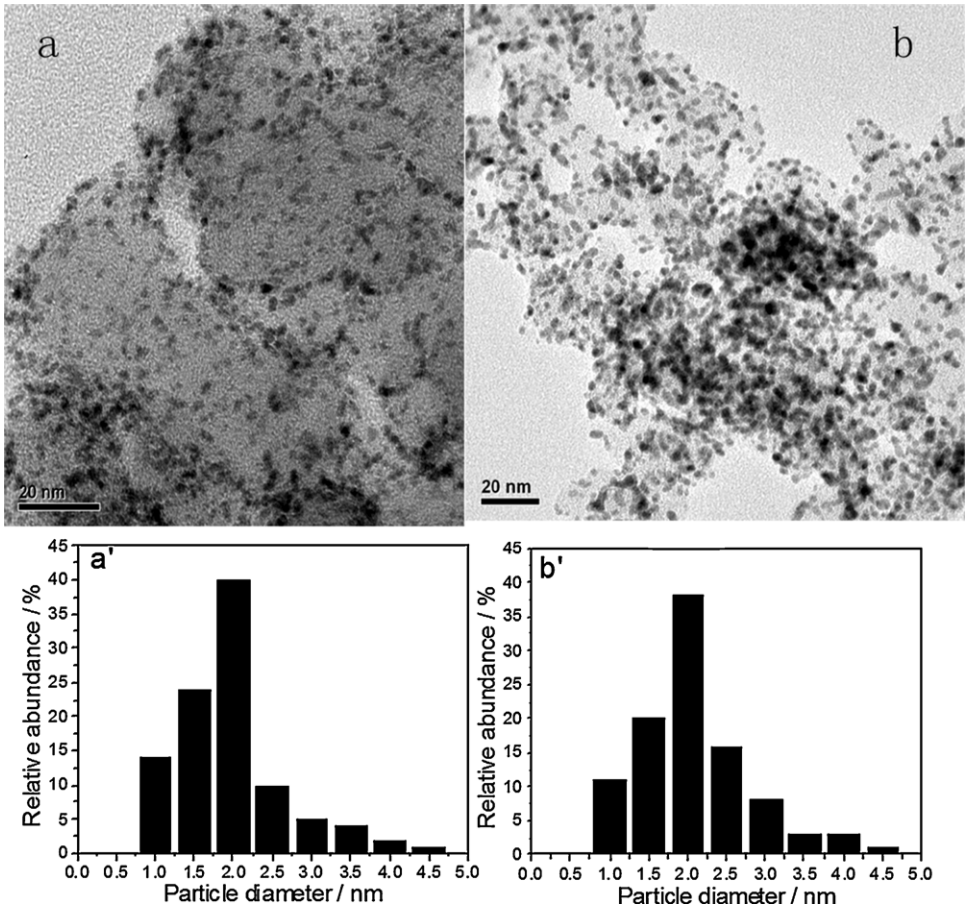

Fig. 10. TEM images of the anode 40% Ir–10% V/C before (a) and after (b) 1010 h testing and histograms of the anode 40% Ir–10% V/C before (a′) and after (b′) 1010 h testing.

For EIS characterization, Nyquist plots for the stack were recorded about every 100 h after 300 h testing and are shown in Fig. 11. For these plots measured at different times, the Nyquist plots were arcs; the high frequency interception on the real impedance axis of the Nyquist plot represents the total ohmic resistance of the cell, which contains the ohmic resistance of the cell components, such as the membrane, catalyst layer, backing layer, and end plate, as well as the contact resistances between each of them. The diameter of the kinetic loop corresponds to the charge transfer resistance associated with the hydrogen oxidation reaction [31]. As revealed in Fig. 11, the ohmic resistance of the stack was almost constant at approximately 5.8 Ω. In contrast, the polarization resistance of the stack changed with operation time. However, no obvious evidence for impedance change can be obtained from the time-dependent plots. Under dynamic loading, both the water and thermal managements inside of the stack become complex, and the balances of water and thermal managements are more difficult than a single cell or a stack running at a constant load. For example, after a full throttle acceleration (from 450 s to 560 s in Fig. 1), if excessive water produced at the cathode side is not properly removed, mass transfer resistance dominates the polarization resistance. At the time of EIS measurement, although the main operation parameters, such as H_2 and air flow, H_2 and air pressure, and coolant temperature and humidification temperature can be controlled, it is difficult to maintain balance among the internal conditions of the membrane, catalyst layer and gas diffusion layer under the stress of dynamically altering water and heat distributions.

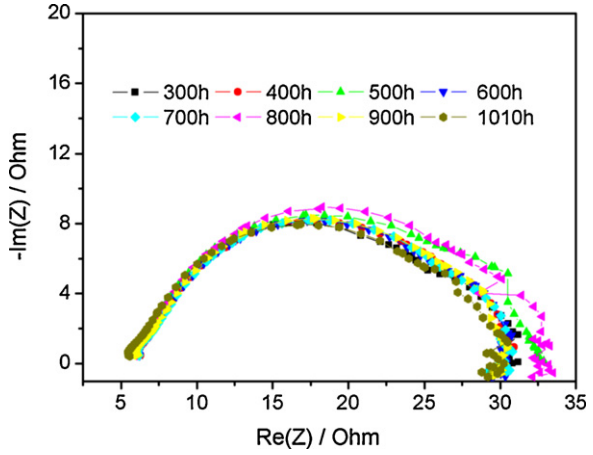

Fig. 11. Electrochemical impedance spectra of the stack.

4. Conclusions

As a substitute for Pt, Ir–V/C binary catalysts with different atomic ratios were prepared. XRD analysis showed that V played an important role in coarsening the Ir particle surface. The optimal ratio of Ir:V, 40% Ir:10% V, was selected based on CVs and LSVs due to its excellent HOR activity and has been used as the anode catalyst in subsequent experiments. A 1.5 kW stack was fabricated and its durability evaluated. For the 1010 h durability testing, an experiment was conducted under a J1015 driving cycle, with 57 start–stops. The stack performance at rated current density decreased only 1.2% within the 1010 h durability test, which was

lower than the 2010 US DOE target. Results from the XRD, TEM, and EIS analyses demonstrated excellent stability of 40% Ir–10% V/C in the fuel cell stack. The enhanced performance of the 40% Ir–10% V/C catalyst in both activity and stability indicate that bimetallic catalysts serve as a promising candidate for practical applications in fuel cell vehicles.

Acknowledgements

The research work was supported by the China MoST (2008AA050403) and in part by Shanghai MoST (10JC1414900), the national "111" project and the Henkel professorship. We also thank Hu Chun for his assistance in experimental procedures.

References

[1] B.K. Prater, J. Power Sources 51 (1994) 129–144.
[2] G. Escobedo, M. Gummalla, R.B. Moore, FY 2006 Annual Progress Report, 2006, pp. 706–711.
[3] J. Marcinkoski, J.P. Kopasz, T.G. Benjamin, Int. J. Hydrogen Energy 33 (2008) 894–3902.
[4] Y. Wang, K.S. Chen, J. Mishle, S.C. Cho, X.C. Adroher, Appl. Energy 88 (2011) 981–1007.
[5] N. Alonso-Vante, W. Jaegermann, H. Tributsch, W. Honle, K. Yvon, J. Am. Chem. Soc. 109 (1987) 3251–3257.
[6] M. Lefevre, J.P. Dodelet, P.J. Bertrand, Phys. Chem. B 106 (2002) 8705–8713.
[7] C.W.B. Bezerra, L. Zhang, K. Lee, H. Liu, H.J. Wang, J.J. Zhang, Electrochim. Acta 53 (2008) 4937–4951.
[8] T. Hakoda, S. Yamamoto, K. Kawaguchi, T. Yamaki, T. Kobayashi, M. Yoshikawa, Appl. Surf. Sci. 257 (2010) 1556–1561.
[9] A. Ishihara, M. Tamura, K. Matsuzawa, S. Mitsushima, K. Ota, Electrochim. Acta 55 (2010) 7581–7589.
[10] A. Serov, C. Kwak, Appl. Catal. B: Environ. 90 (2009) 313–320.
[11] D.J. Myers, X.P. Wang, FY 2010 Annual Progress Report, 2010, pp. 876–880.
[12] D.A.J. Rand, R.J. Woods, Electroanal. Chem. 55 (1974) 375–379.
[13] L. Cao, G.Q. Sun, Q. Xin, Electrochem. Commun. 9 (2007) 2541–2546.
[14] X. Wang, Y. Tang, Y. Gao, T. Liu, J. Power Sources 175 (2008) 748–750.
[15] K. Lee, J. Zhang, J.J. Zhang, J. Power Sources 165 (2007) 108–113.
[16] K. Lee, J. Zhang, J.J. Zhang, J. Power Sources 170 (2007) 291–296.
[17] T. Xu, H.M. Zhang, Y.N. Zhang, J. Hong, Y.F. Tang, J. Power Sources 194 (2011) 5849–5852.
[18] Y. Takasu, N. Yoshinaga, W. Sugimoto, Electrochem. Commun. 10 (2008) 668–672.
[19] B. Li, J.L. Qiao, D.J. Yang, J.S. Zheng, J.X. Ma, J.J. Zhang, H.J. Wang, Electrochim. Acta 54 (2009) 5614–5620.
[20] J.L. Qiao, B. Li, D.J. Yang, J.X. Ma, Appl. Catal. B: Environ. 91 (2009) 198–203.
[21] B. Li, J.L. Qiao, D.J. Yang, R. Lin, H. Lv, H.J. Wang, J.X. Ma, Int. J. Hydrogen Energy 35 (2010) 5528–5538.
[22] D. Liu, S. Case, J. Power Sources 162 (2006) 521–531.
[23] D.J. Yang, J.X. Ma, L. Xu, Electrochim. Acta 51 (2006) 4039–4044.
[24] G. Liu, H.M. Zhang, J.W. Hu, Electrochem. Commum. 9 (2007) 2643–2651.
[25] K. Zhang, Q.L. Yue, G.F. Chen, Y.L. Zhai, L. Wang, H.S. Wang, J.S. Zhao, J.F. Liu, J.B. Jia, H.B. Li, J. Phys. Chem. C 115 (2011) 379–389.
[26] H.T. Duong, M.A. Rigsby, W.P. Zhou, A. Wieckowsk, J. Phys. Chem. C 111 (2007) 13460–13465.
[27] V. Radmilovic, H.A. Gasteiger, P.N. Ross, J. Catal. 154 (1995) 98–106.
[28] R. Borup, J. Meyers, B. Pivovar, Y.S. Kim, R. Mukundan, Chem. Rev. 107 (2007) 3904–3951.
[29] B.J. Eastwood, P.A. Christensen, R.D. Armstrong, N.R. Bates, J. Solid State Electrochem. 3 (1999) 179–186.
[30] X.P. Wang, R. Kumar, D.J. Myers, Electrochem. Solid State Lett. 9 (2006) A225–A227.
[31] C.S. Kong, D.Y. Kim, H.K. Lee, Y.G. Shul, T.H. Lee, J. Power Sources 108 (2002) 185–191.